JOURNAL OF SOLID STATE CHEMISTRY 74, 295–303 (1988)

Short-Range Order in Barium Hexaaluminate (Phase I) Single Crystals

ANDRÉE KAHN, TOMÉ GBEHI, JEANINE THERY, AND JEAN-JACQUES LEGENDRE

Chimie Appliquée de l'État Solide, U.A. 302 CNRS, ENSCP, 11 rue Pierre et Marie Curie, 75231 Paris Cedex 05, France

Received December 7, 1987

Single crystals of barium hexaaluminate (phase I, barium β-alumina) with the composition $Ba_{0.68}Al_{11}O_{17.18}$ have been obtained by zone melting. X-ray and electron diffuse scattering give evidence of local ordering between Ba and vacancies. This short-range order is simulated by a Monte Carlo-type routine and can be described as a two-dimensional superstructure $a\sqrt{3} \times a\sqrt{3}$, covering about 60 Å and limited by zones which contain vacancies or barium clusters.

Introduction

For quite a long period, barium hexaaluminate was given the $BaAl_{12}O_{19}$ formula, corresponding to the magnetoplumbite structure, which generally occurs in divalent-ion hexaaluminates (*1*). During the last decade, however, many studies devoted to this family of compounds revealed that this ideal description was not correct: the true composition range is from 0.8 to 1.3 BaO for $6Al_2O_3$. Moreover, two different phases have been identified, phase I (ϕI) with low barium content and phase II (ϕII). Phase I has a β-alumina-type structure (*2–5*).

The main feature of this structure is its hexagonal symmetry, ($P6_3/mmc$ space group), and Ba atoms are gathered in some specific layers of the host lattice (Fig. 1). Therefore, one can expect vacancies or excess of barium, resulting from the actual composition, more or less disordered on the hexagonal network of Ba sites.

We have prepared single crystals of Ba ϕI phase with a definite composition, for which both X-ray and electron diffraction patterns give evidence of strong diffuse scattering together with the expected Bragg diffraction. This suggests the presence of short-range order superimposed on the average structure of this barium aluminate.

The purpose of this work was to find an interpretation of the diffuse scattering, in relation with this possible short-range ordering between occupied and vacant sites of barium.

Short-Range Order and Diffuse Scattering

Diffraction is expected in crystals with long-range order, i.e., infinite correlation distance. In other terms, this means that knowing the arrangement in a given point of the crystal lattice, it is possible to deduce the arrangement on any lattice point.

Whenever a local organization takes place, diffuse spots or lines are observed on the diffraction patterns, in addition to the

0022-4596/88 $3.00

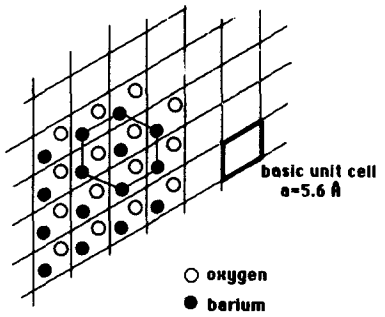

FIG. 1. Schematic description of mirror planes in β-alumina-type structure.

Bragg spots (*6*). Several phenomena can produce diffuse scattering, such as:

(a) Atomic shifts arising from electron–phonon interaction; this results in patterns where diffuse scattering exhibits increasing intensity when going from the center (Bragg angle = 0°) to the outer part of the diagrams. This is generally observed in IVB and VB transition metal dichalcogenides (*7*).

(b) Static substitution disorder, where the diffusion arises from a partial and local organization of atoms (in binary alloys for instance), or of vacancies (in nonstoichiometric compounds). The diffuse scattered intensity then decreases from the center to the outer part of the patterns. This was described, for instance, in $Ti_{1+x}S_2$ (*8*).

Both types of disorder may coexist in the same phase, resulting in a more complex diffraction pattern.

Experimental

(*1*) *Crystal Growth*

Single crystals are prepared by a zone melting process in an arc-image furnace, operating at 1950°C and starting from rods sintered at high temperature (1500–1600°). After repeated zone melting this method provides crystalline rods of a few millimeters in diameter and several centimeters in length. These have easy cleavage planes perpendicular to the hexagonal *c* axis and parallel to the growth axis. The final composition of all such crystals was established by electron microprobe analysis and is close to $Ba_{0.68}Al_{11}O_{17.18}$ (*9*), in spite of variable starting proportions of oxide mixtures.

(*2*) *Diffuse Scattering Evidence*

The experimental device to observe X-ray diffuse scattering has been previously reported (*10*). Let us recall the basic principles of the method:

—the crystal and films are stationary;

—strictly monochromatic radiation is used (here $\lambda \mathrm{Mo}K\alpha$ = 0.7107 Å);

—the transmission pattern is obtained after several days exposure and shows the reciprocal layers perpendicular to the X-ray beam.

All diffraction patterns obtained from crystalline platelets of phase ϕI show the same aspect when the X-ray beam is aligned with the *c* hexagonal axis (Fig. 2). Then diffuse scattering appears in [00.*l*] planes as periodic hexagonal rings, with some reinforced diffuse spots; no diffusion is found where true diffraction occurs. We will then handle the problem in a two-dimensional lattice.

Samples with the same origin were also examined by electron microscopy and their electron diffraction patterns exhibit diffuse spots and lines with the same localization with respect to Bragg diffraction (Fig. 3).

In our case, for the first reciprocal unit cells, it seems reasonable to assess that diffuse scattering originates mainly from a substitution ordering of Ba and vacancies on their sites in the mirror planes of the structure.

Interpretation of Extra Spots

Starting from the *average reciprocal lattice* derived from the Bragg spots, it is pos-

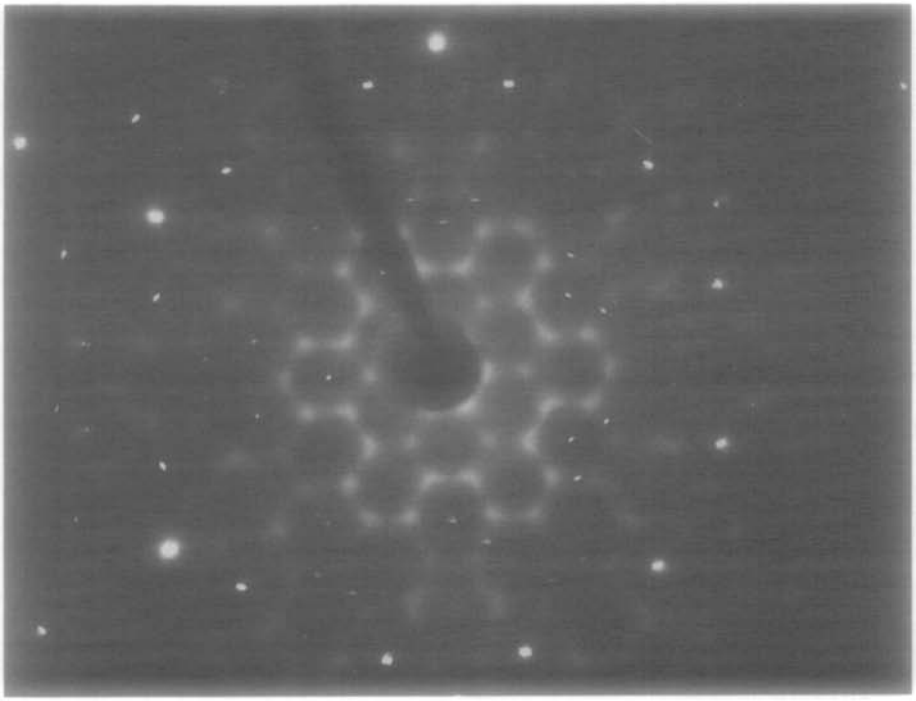

FIG. 2. X-ray diffuse scattering pattern of $\phi 1$ Ba hexaaluminate.

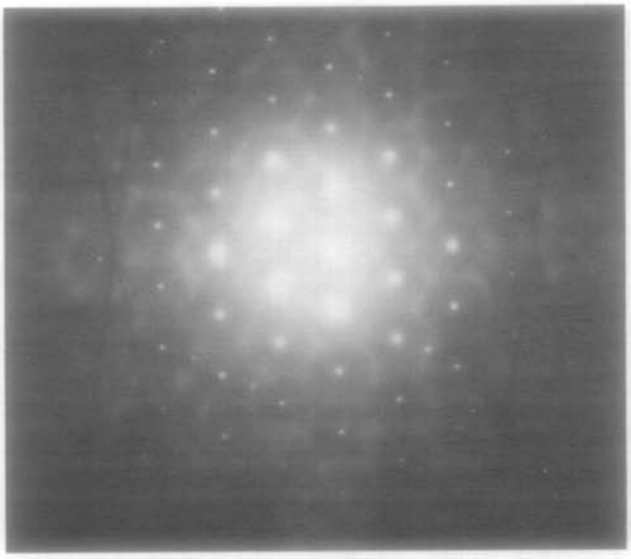

FIG. 3. Electron diffraction pattern of $\phi 1$ phase (JEOL 2000FX).

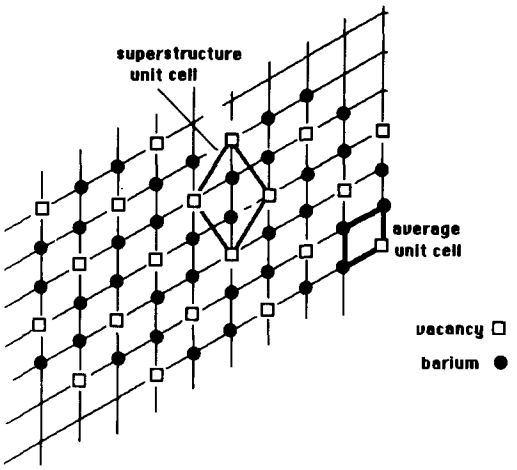

FIG. 4. Two-dimensional superstructure $a\sqrt{3} \times a\sqrt{3}$, for 2 Ba/1 vacancy on a hexagonal lattice.

sible to define a new reciprocal lattice, by assuming the intense diffuse spots at the vertices of hexagonal rings to be diffraction spots (which they are not in fact). This corresponds in real space to a superstructure for which the unit cell is related to the average structure by the following relationships (Fig. 4):

—if a and b are the lattice constants of the basic hexagonal unit cell, the superstructure cell is $a\sqrt{3} \times a\sqrt{3}$ and turned by 30°.

—this supercell contains 3 Ba^{2+} sites of which one is vacant, according to the composition (0.67 Ba instead of 1).

Corresponding to this superstructure cell, a possible ordering scheme is given: every third Ba site is vacant on the basic Ba lattice. This can also be described as a honeycomb of Ba hexagons centered by a vacancy. Then, instead of an average 2D lattice (*P6mm*) where Ba sites are statistically occupied by $\frac{2}{3}Ba^{2+}$, we have a supercell with a vacant site in (0,0) and two Ba in ($\frac{1}{3}$, $\frac{2}{3}$) and ($\frac{2}{3}$, $\frac{1}{3}$) positions (Fig. 4).

In such a superstructure, any Ba site has six nearest neighbors of which three are occupied and three are vacant. In a statistical nonstoichiometry, for six sites, two would be vacant and four occupied, according to the composition (Fig. 5).

Diffuse spots and Bragg spots are indexed in the same 2D reciprocal superstructure lattice. An evaluation of corresponding diffuse scattered intensity I_d is given by the relationship:

$$I_{d_{hk}} = |F_{hk} - \langle F_{hk} \rangle|^2 \ (11),$$

with F_{hk} = structure factor of an ordered model (two-dimensional supercell) and $\langle F_{hk} \rangle$ = structure factor of a statistical model (two-dimensional supercell). In the new lattice, Bragg spots have indexes ruled by the condition:

$$2h + k = 3n \ (n \in Z)$$

and I_d is always found as zero for those spots, as expected from experimental patterns.

Taking the extra spots as superstructure spots, we then have a long-range ordered model, which does not yet account for the diffuse nature of extra spots and lines. This problem is treated in the next section.

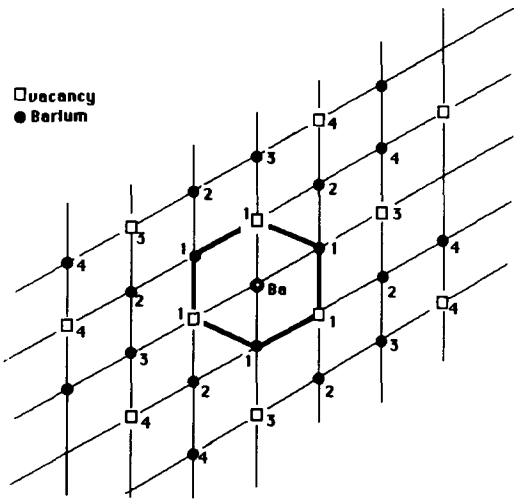

FIG. 5. Count of successive neighbors of a site in a hexagonal 2D lattice.

TABLE I

ORGANIZATION OF THE COMPUTING ROUTINE FOR MODELING SHORT-RANGE ORDER

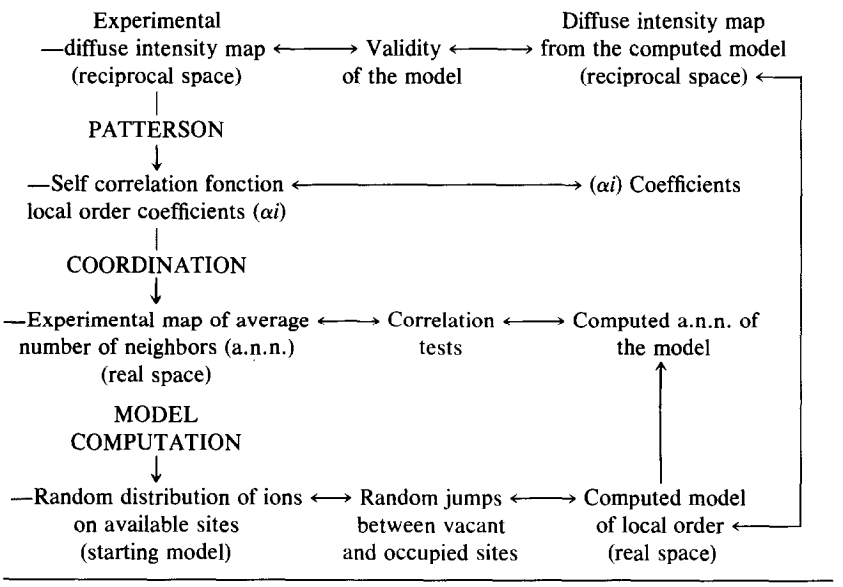

Short-Range Ordering

In order to study the local order, i.e., organization in microdomains, we have used a direct method, previously designed in our laboratory, to study short-range order in nonstoichiometric titanium disulfides (*12*).

It is a computerized *trial and error method,* based on a Monte Carlo calculation. It leads to a computed structural model, starting from raw experimental diffused intensities, average site lattice, and phase composition. This interpretation is derived from calculation of short-range order parameters, assuming an ideal location of diffuse intensity. It works in three distinct steps, which are described in Table I:

(1) From a generalized Patterson function performed with experimental diffuse intensities, short-range order coefficients—Cowley coefficients (*13*)—are computed and the average number of neighbors (a.n.n) in our compound is deduced. This gives the coupling probabilities of atoms in our structure.

(2) A computed model, consistent with this experimental map of neighbors, is built.

(3) The validity of this model is tested by comparison of the Fourier transform of the computed model with the experimentally recorded diffuse intensities.

The main points of each step are reported hereafter.

(*1*) *Exploitation of Experimental Diffuse Scattering*

On the diffuse scattering patterns (reciprocal lattice), it is possible to account for the diffusion by a set of points where an estimated value of intensity is attached to coordinates u, v (Fig. 6).

Then a two-dimensional domain is defined, involving the maximum number of neighbors to be considered for a given Ba site, on the hexagonal Ba network. Here it

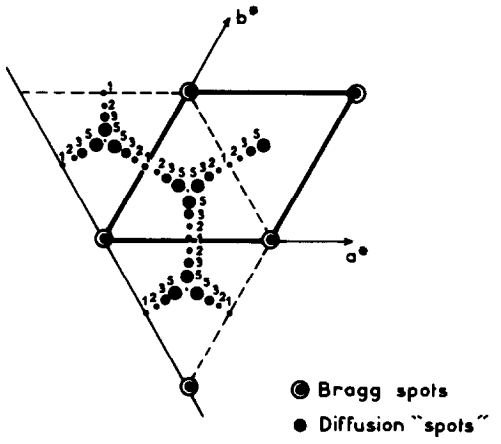

FIG. 6. Schematic description of diffuse scattering data.

includes the 28th neighbor, owing to the size of details on the diffusion pattern.

By means of a generalized Patterson function, we get the successive α_i and lower indices $\alpha 1$, $\alpha 2$, . . . , $\alpha 28$ coefficients for short-range order in our compound. Let us recall here that $\alpha 1$, for instance, is given by

$$\alpha_1 = 1 - (P_{\text{eff}}/P_{\text{stat}}),$$

where P_{eff} is the probability of finding Ba/vacancy pairs in a structure with local order, P_{stat} is the probability of finding Ba/vacancy pairs in a statistical structure with $\frac{1}{3}$ vacancies on the lattice (our example). Then, in a general case:

—if $\alpha_1 < 0$, the structure tends to barium-vacancy pairs, i.e., ordering;

—if $\alpha_1 > 0$, the structure tends to clustering of Ba–Ba or vacancy–vacancy, i.e., segregation of the two species;

—if $\alpha_1 = 0$, the organization is statistical, ruled by the concentration of vacancies.

In Table II the resulting values of average number of neighbors (a.n.n.) in our compound are given; they are compared to the theoretical values expected:

(a) in a random structure with $\frac{1}{3}$ vacancies and $\frac{2}{3}$Ba;

(b) in a long-range ordered superstructure as the one described in the first part of this paper.

The values of our phase range between those two lists (except for the 7th neighbor, which will be explained later on).

(2) *Computing a Short-Range Order Model*

The second step deals with simulation of a computed model of short-range order between Ba and vacancies, which exhibits the same "map of average number of neigh-

TABLE II

COMPARISON OF THE EXPERIMENTAL SUCCESSIVE NUMBERS OF NEIGHBORS TO THE THEORETICAL ONES

Full structure (1 Ba)		Structure with 0.67 Ba	
Number of *n*th neighbors	Random structure	Experimental number of neighbors	Long-range ordered structure
1st neighbor 6	4	3.27	3 Ba + 3 lac.
2nd neighbor 6	4	4.77	6 Ba
3rd neighbor 6	4	4.00	3 Ba + 3 lac.
4th neighbor 12	8	6.79	6 Ba + 6 lac.
5th neighbor 6	4	4.06	6 Ba
6th neighbor 6	4	4.32	6 Ba
7th neighbor 12	8	**8.69**	6 Ba + 6 lac.
28th neighbor 12	8	7.80	6 Ba + 6 lac.

NUMBER OF JUMPS = 15001
NUMBER OF SITES = 1536
NUMBER OF ATOMES = 1024
AGREEMENT FACTOR = 0.0234

Average number of neighbors :

Obs.	Calc.	Obs.	Calc.
3.12	3.35	3.02	3.01
4.81	4.73	6.22	6.57
3.62	3.53	6.02	6.03
6.28	6.68	8.10	8.07
4.00	4.06	3.18	3.03
4.02	3.92	2.99	2.88
7.66	7.50	7.49	7.27
3.14	3.21	5.84	5.83
6.60	6.74	5.49	5.52
6.85	6.87	5.96	6.16
4.16	4.03	5.61	5.72
3.57	3.36	4.02	3.94
7.81	7.59	7.65	7.50
6.17	6.17	5.62	5.45

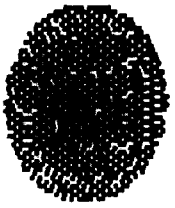

FIG. 7. Computed model for short-range order in phase I.

bors" as that deduced in the previous step.

Starting from a *random distribution* of $2N/3$ Ba on N possible sites on a hexagonal grating, a Monte Carlo routine works by exchanging Ba and vacancy in a pair, repeating these jumps a great number of times in order to fit the experimental α's. These exchanges modify the environment of a given site, and the corresponding average number of neighbors is computed. A fitting test is done at regular intervals (here after every 500 jumps) to compare the experimental a.n.n. and those of the computed model. When the reliability factor R seems stationary, the model no longer improves and is taken as one possible description of local order between Ba ions and vacancies.

Further experimental details are given in Fig. 7:

—The starting array consists of 36 × 36 or 48 × 48 sites; it has to be larger than the environment explored for computing the experimental α_i, and not too large so as to avoid too long a computing time (36 × 36 = 1296 sites).

—The number of jumps ranges between 10^4 and 2.10^4 before getting a steady value of R factor, about 0.025.

The final model is either plotted (Fig. 7) or filed as an array of 1 and 0 (1 = occup. site, 0 = vac.).

(3) Testing the Consistency of the Model

The last section deals with the validity of this model for short-range order. A Fourier transform is performed with the computed model and provides the corresponding distribution of diffused intensities. If compared to the diffuse scattering data originally introduced (Fig. 6), it appears that intensity does occur where it is expected, in the "Bragg" lattice, with correct hexagonal symmetry and reinforced spots at $(\frac{1}{3}, \frac{2}{3})$ and $(\frac{2}{3}, \frac{1}{3})$ positions in the average reciprocal cell (Fig. 8).

Description of Short-Range Order

The model of Fig. 9 is considered as the best one, with regard to the agreement between experimental and simulated average number of neighbors (R = 0.0234) and to the distribution of diffuse intensity. It is in fact straightforward derived from the array of occupied/vacant sites plotted on a hexagonal lattice.

This computed model consists of ordered domains covering a few unit cells. The limits are disrupted zones where clusters of vacancies or of Ba sites are found.

A closer look at the ordered regions reveals that they are made of Ba hexagons with vacancy in their center; this organization is exactly the one described as the pos-

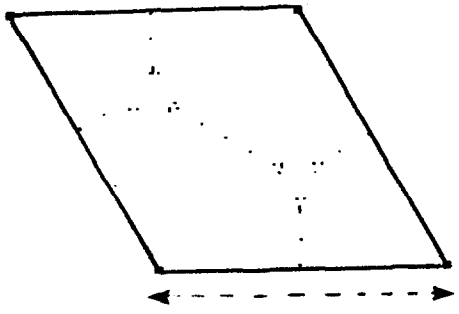

FIG. 8. Fourier transform of the computed model, giving diffuse intensities in the reciprocal unit cell.

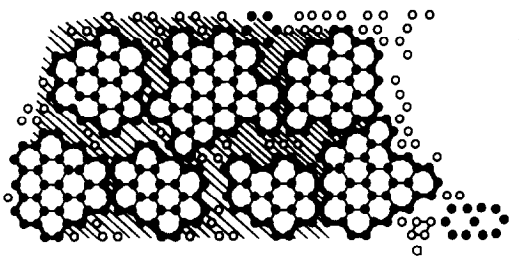

FIG. 9. Modeling of short-range order, showing the ordered zones, edged by regions of Ba or vacancy clustering.

sible long-range order with $a\sqrt{3} \times a\sqrt{3}$ unit cell.

These ordered regions stretch as far as the 7th neighbor (more or less); this could explain the unexpected high value for this average number of 7th neighbors that we found previously (see Table II) since, after the 7th neighbor, the consistency of local organization is lost.

The validity of that description also leans on the following points:

—If either our description of experimental diffuse scattering or the assumed barium concentration is varied, the resulting computed models are not consistent with experimental data. For a higher Ba content for instance, the model exhibits segregation into large domains, some with $a\sqrt{3} \times a\sqrt{3}$ superstructure, some with total disorder.

—The ordered domains occurring in the "good" models are always within the range of the analyzed region (<28th neighbor) and their size (50–60 Å) corresponds to the one deduced from the width of diffused spots and stripes by the Scherrer formula (*14*):

$$L = k\lambda/\Delta\cos\theta,$$

where k is a constant of the diffracting device (60 mm), λ is the X-ray wavelength Mo$K\alpha$, 0.7107 Å; Δ is the width of diffusion spots, 1 mm; θ is the Bragg angle in the considered region (15°).

With these values, L is found to be around 44 Å.

With regard to these features the simulated model of short-range order in Ba ϕI looks consistent.

Some improvements are yet required to get a more comprehensive description of local arrangement. They are:

—quantitative evaluation of diffuse scattering intensities;

—increased computing time to extend the number of neighbors;

—correction of edge effect (on the edges, the statistical number of neighbors is not correct). This is already corrected in the routine and the influence is not negligible. Exploring circular domains within the hexagonal unit cell is a way to reduce the edge effects and it is already done in the computation. A larger explored domain would also minimize these effects. With such better conditions we hope to improve our description.

Meanwhile, our model accounts qualitatively for a local organization in ϕI Ba hexaaluminate. On the 2D (a × a) hexagonal lattice of barium sites, $\frac{2}{3}$ of Ba and $\frac{1}{3}$ of vacancies are locally ordered in a superstructure $a\sqrt{3} \times a\sqrt{3}$, covering a few unit cells (50 Å). These ordered regions are separated by perturbated zones, containing clusters of Ba or of vacancies, which do not exhibit the same environment as in the ordered zones.

Conclusion

We have been able to observe X-ray diffuse scattering in ϕI Ba hexaaluminate with low barium content (0.68 Ba in a β-alumina-type structure). This can be related to a short-range order between Ba and vacancies, on the Ba 2D hexagonal network. This local ordering consists of limited domains of superstructure, spread over 50 Å, and edged by zones with modified environments made of Ba or vacancy clusters.

Other authors have published electron diffraction patterns of βBa ϕI where no diffuse scattering could be detected (*15*).

This main discrepancy with our results is probably due to the difference of chemical composition of their samples: their crystals have a higher Ba content ($Ba_{0.78}Al_{10.9}O_{17.14}$), which does not favor the creation of such ordered domains as those we handle ($a\sqrt{3}$ hexagonal superstructure).

Acknowledgments

We want to thank Dr. G. Dhalenne for help in crystal growth, Professor R. Portier for electron microscope investigation, and Dr. V. Maurice for introducing us to the Monte Carlo routine he had used for surface reaction analysis.

References

1. K. KATO AND H. SAALFELD, *N. Jb. Miner. Abh.* **109**(3), 192 (1968).
2. A. L. N. STEVELS, *J. Lumin.* **17,** 121 (1978).
3. F. HABEREY, G. OEHLSCHLEGEL, K. SAHL, *Ber. Dtsch. Keram. Ges.* **54,** 373 (1977).
4. N. IYI, Z. INOUE, S. TAKAKEWA, AND S. KIMURA, *J. Solid State Chem.* **52,** 66 (1984).
5. N. IYI, Z. INOUE, S. TAKAKEWA, AND S. KIMURA, *J. Solid State Chem.* **60,** 41 (1985).
6. A. GUINIER, "Théorie et technique de la radiocristallographie," p. 490, Dunod, Paris (1964).
7. C. B. SCRUBY, P. M. WILLIAMS, G. S. PARRY, *Philos. Mag.* **31,** 255 (1975).
8. R. MORET AND M. HUBER, *J. Phys. C* **38,** C7 (1977).
9. T. GBEHI, Thèse de doctorat, Universite Paris VI (1987).
10. R. COMES, M. LAMBERT, H. LANNOIS, AND H. R. ZELLER, *Phys. Rev. B* **8**(2), 571 (1973).
11. A. GUINIER, "Théorie et technique de la radiocristallographie," p. 502, Dunod, Paris (1964).
12. J. J. LEGENDRE AND M. HUBER, *J. Appl. Crystallogr.* **13,** 193 (1980).
13. J. M. COWLEY, "Diffraction Physics," North Holland, Amsterdam (1975).
14. A. GUINIER, "Théorie et technique de la radiocristallographie," p. 464, Dunod, Paris. (1964).
15. N. IYI, S. TAKEKAWA, Y. BANDO, AND S. KIMURA, *J. Solid State Chem.* **47,** 34 (1983).